Stepwise artificial yarn muscles with energy-free catch states driven by aluminum-ion insertion

Ming Ren [a,b], Panpan Xu [b], Yurong Zhou [a,b], Yulian Wang [a,b], Lizhong Dong [a,b], Tao Zhou [c], Jinke Chang [e], Jianfeng He [a,b], Xulin Wei [b], Yulong Wu [b], Xiaona Wang [b], Wei Chen [d], Jiangtao Di [a,b,c], * and Qingwen Li [a,b,c] *

[a] School of Nano-Technology and Nano-Bionics, University of Science and Technology of China, Hefei 230026, China

[b] Key Laboratory of Multifunctional Nanomaterials and Smart Systems, Advanced Materials Division, Suzhou Institute of Nano-Tech and Nano-Bionics, Chinese Academy of Sciences, Suzhou 215123, China

[c] Division of Nanomaterials and Jiangxi Key Lab of Carbonene Materials, Jiangxi Institute of Nanotechnology, Nanchang 330200, China

[d] Research Centre for Smart Wearable Technology Institute of Textiles and Clothing, The Hong Kong Polytechnic University, Kowloon, Hong Kong 999077, China

[e] Division of Surgery and Interventional Science, University College London, London NW3 2PF, UK

E-mail: jtdi2009@sinano.ac.cn, qwli2007@sinano.ac.cn

ABSTRACT: Present artificial muscles have been suffering from poor actuation step precision and the need of energy input to maintain actuated states due to weak interactions between guest and host materials or the unstable structural changes. Herein, these challenges are addressed by deploying a mechanism of reversible faradaic insertion and extraction reactions between tetrachloroaluminate ions and collapsed carbon nanotube. This mechanism allows tetrachloroaluminate ions as a strong but dynamic "locker" to achieve an energy-free high-tension catch state and programmable stepwise actuation in the yarn muscle. When powered off, the muscle nearly 100% maintained any achieved contractile strokes even under loads up to 96,000 times the muscle weight. The actuation mechanism allowed the programmable control of stroke steps down to 1% in during reversible actuation. The isometric stress generated by the yarn muscle (14.6 MPa in maximum, 40 times that of skeletal muscles) was also energy-freely lockable and step controllable with high precision. Importantly, when fully charged the muscle stored energy with a high capacity of 102 mAh g^{-1}, allowing the muscle as a battery to power secondary muscles or other devices.

INTRODUCTION

Bivalve mollusks can keep their hard shells tightly closed while consuming very low energy. This muscle behavior is known as the catch state, which is enabled by Ca^{2+}-regulated trimeric compounds formed by actin filaments and myosin filaments in the anterior byssus retractor muscle.[1, 2] Endowing artificial muscles with a catch state is extremely important because it allows the retention of tensioned actuation states without continuous stimulations and energy consumption, and programmable stepwise actuation according to control profiles. Till now, various artificial muscles that can reversibly contract, bend, expand, or rotate when subjected to external stimuli have been developed.[3-5] However, such a catch state featuring energy-free high actuation retention and stepwise actuation has rarely been achieved yet.

This deficiency is mainly limited by the actuation mechanism of the presently developed artificial muscles. Generally, artificial muscles perform based on stimulus-induced volume changes,[6, 7] which can be achieved mainly by such means as temperature difference,[8-10] electrostatic pressure,[11-13] and guest materials interactions.[14-16] When heated by the Joule effect or external heaters, fibers of highly oriented semicrystalline polymer or carbon nanotube (CNT)/elastomers can generate large contractile strokes and high power density (e.g. 49% stroke by nylon fibers[8], 2.15 J g^{-1} contractile work capacities by sheath run muscles[17]). However, the keep of contracted states with a high retention ratio needs continuous heat input due to heat dissipation. For example, a nylon fiber rapidly decayed by 65% in contractile stroke and 88% in stress, respectively, when powered off.[18] Dielectric elastomer films, such as silicone elastomers (polydimethylsiloxane,[19] or Ecoflex 00-30[20]) can produce fast and large strains when a high voltage is applied to the two sides of the films. Since the structure deformation is caused by

electrostatic pressure, a high voltage is necessary to maintain the stained states.[6, 12, 21] Actuation mechanisms based on the infiltration and evaporation of solvents or vapor and the electrochemical injection and extraction of ions are closely related to the interactions between the guest materials and the artificial muscles. Infiltration and extrusion of hierarchical CNT yarns,[15] graphene oxide fibers,[22] cotton fibers,[23] and PEO-SO$_3$/CNT yarns[17] by solvents have resulted in actuation actions in the forms of contraction, bending, or rotation depending on the muscle structure. Due to the evaporation and tension-induced extrusion of the solvents, the actuation retention of such artificial muscles needs a solvent-rich environment as the continual stimulation.[24] Artificial muscles by electrochemical injection and extraction of ions feature low driving voltages and high actuation strokes. The realization of a catch state in such electrochemical artificial muscles is highly dependent on the interaction strength between ions and the artificial muscles. Electrochemical artificial muscles by double-layer charging lose the generated force and displacement very quickly when powered off,[25] possibly due to the extrusion of ions and electrolytes out of the muscle by the accumulated tension in the muscle. Artificial muscles driven by electrochemical redox reactions could have a moderate catch state due to the enhanced ion-muscle interaction.[26] We previously reported that the CNT/graphene oxide hybrid muscle yarn when operated in an aqueous electrolyte showed good contraction retention after power off. However, the contractile stroke of this muscle was only 6% and the stepwise actuation is not available.

Based on these considerations, a strong but dynamic "locker" that is energy-free should be built in an artificial muscle to retain the actuation state and allow programable actuation especially when the artificial muscle is actuating under a heavy load. Here, we proposed a new strategy that utilizes intercalation compounds that formed during an electrochemically reversible insertion reaction to well hold the CNT yarn muscles at any achieved stroke. AlCl$_4^-$ anions were faradaically

and quantitively inserted in the collapsed CNT yarn muscles to form the intercalation compounds, resulting in a novel catch state during a long period as well as precious control of contraction at very small strain steps. This new actuation mechanism also allows the energy-free maintenance of high contractile forces generated by the muscles. Resulting from the insertion reaction nature, the muscles stored high electrical energy, which was utilized for powering electronics and other muscles.

RESULTS AND DISCUSSION

Preparation and characterization of artificial muscles. Figure 1a shows a mussel in a closed and open state, as well as a simplified mechanism for understanding the catch state of the muscle in the mussel. The mussel can remain in a close and open state with low energy consumption due to the Ca^{2+}-regulated bonding between actin filaments and myosin filaments. When the Ca^{2+} binds to the myosin neck, the myosin attaches to the actin filament and dephosphorylated twitchin, and a trimeric compound is formed resulting in the catch state.[2]

Inspired by the trimeric compounds-enabled catch state, we introduce an intercalation compound formed by $AlCl_4^-$ anions and collapsed CNT yarn to allow stepwise actuation and actuation catch state in an artificial muscle. Figure 1b shows the presently utilized reaction system for actuation, which is an electrochemically reversible insertion and extraction reaction. The system consists of a coiled CNT artificial yarn muscle as the cathode, a thin Al plate as the anode, and an ionic liquid of $AlCl_3$/1-ethyl-3-methylimidazolium chloride ([EMIm]Cl) as the electrolyte. The reactions involved in the charging and discharging process were shown in Figure 1b[27, 28]. On the cathode side: $C_n + AlCl_4^- \leftrightarrow C_n[AlCl_4] + e^-$, $AlCl_4^-$ ions are inserted into the collapsed CNT yarn and form a compound of $C_n[AlCl_4]$, where n is the molar ratio of carbon atoms to $AlCl_4^-$ in

the CNT yarn.[27] During discharging, $AlCl_4^-$ ions are reversibly extracted out from the yarn. On the anode side, the reaction of $4Al_2Cl_7^- + 3e^- \leftrightarrow Al + 7AlCl_4^-$ occurs correspondingly.

Notably, the insertion of $AlCl_4^-$ resulted in the radial volume expansion of the coiled CNT yarn, which generated the untwisting torque and pulls the coils together. And the radial volume expansion was transformed into the axial contraction to generate the axial contraction of the coiled CNT yarn. When the $AlCl_4^-$ were extracted from the coiled CNT yarn, the axial contracted CNT yarn returned to the original length.[8,29] Figure 1c shows the axial contraction and restoration of a coiled yarn muscle during the charge and discharge process. Like trimeric compound formed between actin filaments and myosin filaments, the intercalation compound endows the coiled yarn muscle with a novel catch state. The coiled yarn muscle holds the achieved contraction states after turning off the energy input either during the charge or discharge process. The catch state also resulted in an important property that the coiled yarn muscle can be stepwise actuated.

Presently used CNT yarns were prepared by floating catalytic chemical vapor deposition.[30] Figure 2a shows the scanning electron microscopy (SEM) image of an 88-μm-thick twisted CNT yarn that has a bias angle of 33°. After counterclockwise twisting the yarn with a twist density of 25000 turns m^{-1} (Figure S1 in the Supporting Information), a coiled CNT yarn with a reduced fiber diameter of 65 μm was formed (Figure 2b), which was used as the artificial muscle. The stress-strain curves show the breaking strengths of CNT yarn were decreased from 129 MPa to 99 MPa during the twisting process. The percentage of elongation at break was 23% and136% before and after twisting, respectively (Figure S2 in the Supporting Information). Cross-sectional transmission electron microscopy (TEM) image of the coiled yarn shows that the CNTs typically have 2-3 graphitic walls and a large number of CNTs are collapsed with a typical "dog bone" shape and stacked in a "dislocation-dipole" mode (Figure 2c).[31] However, there are still a small amount

of multi-walled CNTs (the graphitic walls > 3) that have not collapsed (Figure S3 in the Supporting Information). In defect-free CNTs materials, it is challenge for $AlCl_4^-$ to permeate into the CNTs due to the large size of $AlCl_4^-$. While the interlayer spacing between collapsed CNTs was 0.37 nm, almost identical to the graphite (002) space (0.34 nm). This collapsed stacking structure can provide transportation channel and space for $AlCl_4^-$ storage like a graphite electrode does,[27] which enables the coiled CNT yarn a suitable cathode material for Al-ion batteries.[32]

Figure 2 g shows the typical cyclic voltammetry (CV) curve of a coiled CNT yarn artificial muscle, which was carried out at a scan rate of 1 mV s^{-1} between 0 V and 2.2 V. After the first CV scanning cycle, the CV curves almost coincided (Figure S4 in the Supporting Information), indicating that the electrochemical process became stable and reversible. The oxidation peak at around 2 V during the charging process is associated with the insertion of $AlCl_4^-$ into the collapsed CNT bundles. The reduction peak located at around 1.48 V during the discharging process was due to the $AlCl_4^-$ extracting from the CNT bundles.[32] Figures 2d-f exhibit the TEM image and the high-resolution energy-dispersive X-ray spectroscopy (EDS) elemental mapping of the cross-section of the fully charged CNT yarn. Elements of Al and Cl were observed in the spacing between CNT bundles while they were negligible in the cross-section of wet CNT yarn before being charged (Figure S5 in the Supporting Information). This well indicates the insertion of $AlCl_4^-$ ions into CNT bundles during the charging process.

To further understand the insertion process during the charging and discharging process, ex-situ Wide-Angle X-ray Scattering (WAXS) was performed (Figure S6 in the Supporting Information). Considering the collapsed stacking structure indicated above (Figure 2c), the WAXS peak between 1.2 Å^{-1} to 2.4 Å^{-1} can be fitted into two peaks at q values of 1.684 Å^{-1} and 1.839 Å^{-1} (Figure S7 in the Supporting Information), which can be assigned to the interlayer distance d

value of about 3.73 Å (outer layer distance between adjacent collapsed CNT spacing) and 3.42 Å (interlayer graphitic spacing) based on the TEM results (Figure 2c),[33] respectively. When the yarn was charged, the spacing between the outer layers of adjacent collapsed CNTs increased to 3.79 Å. During the discharging process, the spacing returned to 3.72 Å (Figure S8 in the Supporting Information). The spacing change during the charging and discharging process is consistent with the reversible insertion and de-insertion of $AlCl_4^-$ ions.

In situ Raman spectroscopy was further performed on the CNT yarn to probe the $AlCl_4^-$ insertion and de-insertion during charging and discharging (Figure 2f). The G peak blue-shifted slightly from 1582 cm^{-1} to 1587 cm^{-1} with increasing the voltage from 0 V to 1.7 V, due to the electrostatic absorption of $AlCl_4^-$ ions. When the CNT yarn was charged to 1.8 V, a new peak appeared and overlapped with the D′ peak (at 1614 cm^{-1})[34] (Figure S9 in the Supporting Information). This newly emerged peak was also observed for graphite electrodes that were inserted by $AlCl_4^-$ ions, which has been attributed to the splitting of the G peak due to the rearrangement of positive charges on graphite boundary layers.[35] When the yarn was fully charged at 2.2 V the new peak and the G peak blue-shifted to 1621cm^{-1} and 1596 cm^{-1}, respectively. The G band splitting and the blueshift strongly suggest the strong interactions between the $AlCl_4^-$ ions and CNTs by the formation of intercalation compounds $C_n[AlCl_4]$. During sweeping voltage back to 0 V, the G peak gradually returned to its initial position accompanied by the back-shift of the new peak that finally overlapped with the G peak (Figure S10 in the Supporting Information). The intensity of the D peak located at 1312 cm^{-1} weakened during the charging process and nearly disappeared at a fully charged state and recovered at a fully discharged state. That is due to the reversible resonance conditions during the charging and discharging process.[36]

Actuation performance of aluminum-ion insertion-driven artificial muscle. Figure 3a shows the stabilized time dependence of contractile stroke and current during a full cycle of CV scan between 0 V to 2.2 V at 1 mV s^{-1} for a coiled CNT yarn that was subjected to 12.1 MPa stress. The time dependence of contractile stroke could be roughly divided into three stages as indicated (Figure 3a). At stage I where the voltage increased from 0 V to 1.7 V, the increase of the contractile stroke was relatively small, while the current remained positive and gradually increased. At stage II, the contractile stroke quickly increased from 2.7% at 1.7 V to 18.1% at 2.2 V. This suggests that the insertion of AlCl$_4^-$ ions to form C$_n$[AlCl$_4$] at this voltage range caused a large contractile stroke. At stage III where the voltage decreased from 2.2 V to 0 V, the contractile stroke gradually decreased to 0% due to the reverse reaction (C$_n$[AlCl$_4$] → C$_n$ + AlCl$_4^-$) and the corresponding extraction of AlCl$_4^-$ ions out of the yarn muscle. Even though the current sharply switched from positive to negative and remained large at this stage, the recovery rate was smaller than the contraction rate at stage II. This indicates that the release of AlCl$_4^-$ ions out of the yarn muscles is a relatively slow and potential-dependent process. We integrated the current with time to obtain the charge. The curve of charge versus time during a full CV scan shows the charge increase with time during first 2200 s and decrease in the last 2200 s (Figure S11a in the Supporting Information). The rate of the extracted charge to the injected charge (coulombic efficiency) is about 83% (Figure S11b in the Supporting Information). The coulombic efficiency increase with the scan rate, it reach up 97.3% when the scan rate increase to 50 mV s^{-1} (Figure S12 in the Supporting Information). This might be due to the parasitic reactions under lower scan rate.

To further understand the voltage dependence of the contractile stroke, we measured the contractile strokes of the yarn muscle by doing CV from different starting voltages to 2.2 V and from 0 V to different end voltages at 1 mV s^{-1} (Figure 3b). As shown in the bottom x-axis, in the

voltage ranges of 0–0.3 V, 0–0.6 V, 0–0.9 V, and 0–1.2 V, the yarn muscle nearly did not contract despite the existence of ion injection. This may correspond to a process of drafting $AlCl_4^-$ ions that were stored in the pores of the yarn to the pore surface. This is consistent with the observation of no contraction during the first 1000 s in Figure 3a. When $AlCl_4^-$ insertion that occurred at high voltages (1.7 V–2.2 V) was involved, high contractile strokes were achieved. However, only scanning between the $AlCl_4^-$ insertion-involved voltage ranges (e.g. 1.5–2.2 V, 1.8–2.2 V, or even 1.2–2.2 V) resulted in relatively small contractile strokes (Figure 3b, top x-axis). This can be explained by the relatively slow processes of the reaction ($C_n[AlCl_4] \rightarrow C_n + AlCl_4^-$) and the release of $AlCl_4^-$ ions out from the CNT yarn muscle. Fully extracting the $AlCl_4^-$ ions is thus of great importance for the yarns to return to the initial state. These results suggested that the actuation of CNT yarn muscles is dominated by faradaic $AlCl_4^-$ insertion and extraction with the formation and depletion of intercalation compound $C_n[AlCl_4]$.

We then investigated the dependence of contractile stroke on charges that were injected and extracted from the CNT yarn muscle using CV between 0 V to 2.2 V at different rates of 0.6, 1, and 10 mV s^{-1} (Figure 3c). Importantly, when at low scan rates, the hysteresis of contractile stroke during cycling was very small and the Columbia efficiencies at these scan rates were almost 100%. This suggests that the actuation is highly dependent on the charges that are stored in the muscle and thus the actuation process can be precisely controlled. To investigate the effect of the rate of injected charges on contractile stroke, galvanostatic charging and discharging was further utilized. Figure S13 (Supporting Information) shows the charge dependence of contractile stroke at the current densities of 0.6, 0.8, and 1 A g^{-1}, respectively. The curves were almost coincident.

Figure 3d shows the contractile stroke and the generated contraction work under different applied tensions. The contractile stroke increased first, reached the maximum stroke of 15.6% at

10.6 MPa, and then decreased with the applied stress increased from 13.6 to 24 MPa. When the stress was low, the coil-to-coil distance was limited for contraction.[29] However, too large applied stress would lead to the mechanical injury of the coiled yarn. The maximum contraction work generated by the coiled yarn was 0.88 J g^{-1} at 24 MPa, which is about 22 times that generated by mammalian skeletal muscles.[37] We also investigated the rate performance of the yarn muscle by applying 0 V to 2.2 V square wave voltage with a 50% duty cycle at different frequencies. The largest contraction and recovery rates of the yarn muscles were 5%/s and 12%/s, respectively (Figure S14 in the Supporting Information). The artificial muscle exhibited stable contractile strokes during 1100 actuation cycles in about 13.5 hours when driven by applying CV scan voltage from 0 V to 2.2 V at 100 mV s^{-1} (Figure S15 in the Supporting Information). This indicates the good cyclic stability of the artificial muscle by faradaic $AlCl_4^-$ insertion and extraction.

We further investigated the isometric stress that was generated by the CNT artificial yarn muscle. When the voltage was swept to 2.2 V at 1 mV s^{-1}, the yarn muscle output 14.6 MPa isometric stress (Figure 3e), which is about 40 times than that of skeletal muscles,[38] and much higher than other reported electrochemical artificial muscle (Table S1 in the Supporting Information).[37, 39, 40]. We measured the isometric stress under different applied tensions when the applied voltage scan from 0 to 2.2 V at 50 mV s^{-1}. The isometric stress increased first and then decreased with the increase of applied tensions. The maximum isometric stress is 5.85 MPa at the applied tension of 12.1 MPa (Figure S16 in the Supporting Information). Figure 3f shows that the generated stress was dependent on the voltage on/off frequency. Increasing the frequency and the scan rate led to a decrease in the isometric stress. This could be caused by the limited reaction rate and migration rate of the ions. We further investigated the effect of applied voltage on isometric stress. The isometric stress increased with the increase of applied voltage. The same as the

contractile stroke, when the insertion voltages (1.7 V–2.2 V) were involved, high isometric stress was achieved. The isometric stress was 5.14 MPa at the square wave voltage of 0 V to 1.8 V and increase to 13 MPa when the applied voltage increased to 0-2.2 V (Figure S17 in the Supporting Information).

Novel catch state and stepwise actuation of artificial muscles. Due to the nature of faradaic insertion and extraction, the coiled CNT artificial muscle exhibited a novel actuation catch state and was capable of stepwise actuation. During the CV scan starting from 0 V at 1 mV s^{-1}, we turned off the power when the voltage reached 0.9, 1.2, 1.5, 1.8, and 2.2 V and recorded the contractile stroke versus time (Figure 4a). The yarn muscle that was subjected to 12.1 MPa stress held at the achieved strokes very stably (catch index: ~95.7%) for a period as long as 2000 s after power off. Here a catch index is defined as the ratio of the real-time stroke (or stress) after powering off over the stroke (or stress) achieved just before powering off. Figure 4b shows the contractile strokes that were achieved by applying a series of step voltages. For any given voltages, the power was turned on for 10 seconds and then turned off for 300 seconds. The yarn muscle quickly contracted when the power was on and the catch index was almost 100% during the following 300 seconds. Figure S18 (Supporting Information) summarizes the energy-free catch index for the yarn that was charged to different voltages of 0.9, 1.2, 1.5, 1.8, and 2.2 V and powered off for 300 s and 2000 s. While a slight decrease in the catch index was observed with prolonging the power-off period to 2000 s, the catch index still was as large as 97.7%. To investigate the effect of tension on the catch state, the energy-free contractile retention ratios for the yarn that was charged to 2.2 V under different tension states were characterized (Figure 4c). Surprisingly, the yarn muscle achieved a catch index of about 99% even when bearing a load of 96000 times the muscle weight (30MPa) for 300 s. After the power off for 3600 s, the catch index was still maintained at about

100% under 6 MPa tension load (Figure S19 in the Supporting Information), which is superior to that of previously reported artificial muscles (Table S2 in the Supporting Information).[18, 24, 40-43]

The yarn muscle also showed a novel catch state for the generated isometric stress. As shown in Figure 4d, we charged the yarn at 0.9 V, 1.2 V, 1.5 V, 1.8 V, and 2.2 V for 10 seconds, then turned off the power. The isometric stress generated at voltages lower than 1.8 V was kept almost constant after power off for 300 s. Figure S20a (Supporting Information) shows the catch index of the generated isometric stress. When the voltage was turned off for 300 s, the yarn that was charged at 1.5 V, 1.8V, and 2.2 V exhibited the catch index of about 96%, 92%, and 83%, respectively. The decay rate of the catch index gradually decreases, then reach a plateau of nearly $0\,\%\,s^{-1}$ (Figure S20b in the Supporting Information).

The above-mentioned results indicate that the CNT yarn muscles when driven by faradaic insertion and extraction of $AlCl_4^-$ ions can stably remain contractile strokes and isometric stress without consuming energy. This novel catch state for both stroke and stress was not observed in previously reported well-known artificial muscles, such as shape memory alloy, ionic-polymer/metal composites (IPMCs), dielectric elastomer actuators, and piezoelectric actuators.[6, 26] Since an artificial muscle is generally in a tension state when actuated, energy is needed to prohibit the release of tension. For electrochemical artificial muscles, the actuation retention is thus highly dependent on the reservation of the ions in muscles. Previous work demonstrates that a mechanical stretch can squeeze out ions that are stored in a coiled CNT yarn by double-layer charging, which causes the potential change.[44] This indicates that the master-guest interaction is not sufficiently strong against tension release for artificial muscles based on double-layer charging and discharging.[25] The previously reported CNT muscle yarn that was based on double-layer charging and discharging showed quick decay of catch index when power off, and the catch index was 30%

after power off for 500 s.[40] We also investigated the catch index of a coiled CNT yarn muscle that was driven by double-layer charging and discharging. The catch index of the yarn muscle was about 6% after power off for about 2000 s (Figure S21 in the Supporting Information). In contrast, the insertion of $AlCl_4^-$ ions into the yarns results in the formation of the intercalation compounds of $C_n[AlCl_4]$.[34] This enhances the interactions between the $AlCl_4^-$ ions and CNTs and thus inhibits the tension-induced extrusion of $AlCl_4^-$ ions out of the yarn even when the power is off. The reservation of the $AlCl_4^-$ ions in muscles can be reflected by the good retention of the open-circuit voltage between the yarn muscles and the aluminum plates, especially when the power was turned off below 1.8 V (Figures. 4 a, b, and d). The gradual decrease of the open-circuit voltage at a highly charged state might be due to the parasitic reactions induced by the polarization of electrolytes.[45]

While stepwise actuation has been well achieved in electric motors, the step control of the actuation of artificial muscles is still a challenge. Benefiting from the novel catch state and the charge-regulated actuation of present yarn muscles, we further investigated the stepwise contraction of the yarn muscles. We show in Figure 4e that the yarn muscle achieved stepwise contraction at different modes of 8%, 4%, 2%, and even down to 1%, respectively. This suggests the capability of the programmable actuation control of our yarn muscle. Figure S22 (Supporting Information) showed the utilized voltage profiles for the contraction step control that were obtained according to the charge-contraction relationship (Figure 3a). By using the voltage profiles, the yarn muscle was controlled to contract at very even stroke steps and jumped step by step to the maximum stroke. Further discharging the yarn muscle at programmed voltage caused the yarn muscle to return stepwise to the initial muscle length.

Energy storage by yarn muscles and application. Due to the insertion nature, present artificial muscles can serve as an Al-ion battery to provide electricity. Figure 5a displayed the

galvanostatic charging and discharging at different current densities between 0 V to 2.2 V for the artificial muscle. The specific capacity was about 102 mAh g^{-1} at 400 mA g^{-1} (Figure S23 in the Supporting Information). The specific capacity decreased and the Coulombic efficiency increased with increasing the current density. The specific capacity was maintained at 53.9 mAh g^{-1} and the Coulombic efficiency reached 99.5% at a high current rate of 4 A g^{-1}. Figure S24 (Supporting Information) shows the differential capacitance analyses (dQ/dV) of the galvanostatic charge-discharge curve at 400 mA g^{-1}. The curve exhibited an oxidation peak of around 2 V and a reaction at around 1.45 V, which was consistent with the CV curve (Figure 2g). The coiled yarn displayed a capacity retention of 86% after 260 galvanostatic charge-discharge cycles and the Coulombic efficiency was maintained at 99.5% after 260 cycles (Figure S25 in the Supporting Information).

We demonstrated the utilization of a fully charged yarn muscle (muscle I) as a power source to actuate a secondary yarn muscle (muscle II), as shown in Figure 5c. Figure 5d shows the contractile strokes versus time for muscle I and muscle II when using muscle I to power muscle II. The muscle I was firstly charged to 2.2 V and generated a contractile stroke of 15%. When connected to muscle I, muscle II contracted immediately and then reach a stroke platform of about 4.2%. Correspondingly, the contractile stroke of muscle I decreased by about 1%. The voltage between muscle I and Al anode decreased to about 1.77 V during this process. After charging three times, muscle II contracted by 9.8%. Interestingly, the contractile stroke of muscle II increased by using a multi-ply yarn as muscle I since the capacity of muscle I was increased (Figure S26 in the Supporting Information).

We emphasize the importance of this feature for the utilization of a couple of these yarn muscles to drive the full cycle movement of structures. Previously reported electrochemical yarn muscles needed mechanical stretch to return to the initial muscle length before actuation,[46] which

limited the practical applications of the yarn muscles. The proposed CNT yarn muscles can be a potential solution that is able to utilize the stored energy for muscle recovery. As schematically shown in Figure 5d, an elbow bends and does work when a large-capacity muscle is charged. The large-capacity muscle can power a low-capacity muscle to contract, which makes the elbow return to the initial position (Figure 5b). As another example, we showed the use of the energy stored in a yarn muscle to power a car toy (Figure 5f, Video S1 in the Supporting Information). During charging, the artificial yarn muscle contracted and pulled the car toy forward. The charged artificial yarn muscle was used to power a mini motor for towing the car back and the position recovery of the yarn muscle.

Moreover, the length of the yarn muscle can be utilized to monitor the state of charge (SOC) of the yarn battery. Figure 5e displayed the experimental and fitting curves of the voltage versus the contractile stroke of a fully-charged artificial yarn muscle that was discharged at 0.6 A g^{-1}. The adjusted R-squared of the two fitting curves were both 0.996, which means that the voltage between the CNT coiled yarn and the Al plate could be monitored accurately by the yarn length. This provides a visible battery monitoring mothed to trace the SOC in the yarn muscle. As an energy storage device, the artificial muscle can also be used to power LED lights (Figure 5g, Video S2 in the Supporting Information).

CONCLUSION

In summary, the electrochemical artificial muscles driven by aluminum-ion faradaic insertion and extraction have exhibited an energy-free high-tension actuation catch state and programmable stepwise actuation. This is enabled by the voltage-dependent formation and removal of $C_n[AlCl_4]$ compounds in the CNT yarn muscles, which can act as a strong and dynamic structural locker in

the muscle. This provides a new strategy for solving the long-standing challenge of energy-saving and precise control of artificial muscles. The new driving mechanism also endows the artificial muscles with a high energy storage capability. This can rich the functions of the yarn muscles as position recovery, battery-capacity monitoring, a power source for sensors, and so on. We believe that the new driving mechanism can also inspire the development of novel artificial muscles that have programmable actuation control and low energy consumption.

EXPERIEMENTAL SECTION

Preparation of artificial muscles: CNT yarns were fabricated by floating catalyst chemical vapor deposition.[30] In this method, absolute ethanol serves as a carbon source, ferrocene as catalyst (1-3wt%), thiophene as catalytic aid (2-5%), and deionized water as etchant (2-5%). The H_2/Ar mixed gas serves as carrier gas. The temperature of the growth reaction furnace was 1100 ºC to 1300 ºC. The mixed solution of carbon source was injected into the reaction furnace, and a continuous CNT aerogel sheet was drawn from the end of the furnace. After passing the aerogel sheet through a water tank, narrow CNT ribbons were obtained. The ribbon was twisted at a twist density of 25000 turns m^{-1} under a load of 2 g, which led to the formation of a fully coiled CNT yarn. The coiled yarn was utilized as the artificial muscle.

Electrochemical measurements: The coiled CNT yarn was used as a cathode, the Aluminum plate was used as an anode, and the ionic liquid $AlCl_3$/1-ethyl-3-methylimidazolium ([EMIm]Cl) (mole ration of $AlCl_3$ to [EMIm]Cl was 1.3) was used as electrolyte. Raman spectroscopy shows that both $AlCl_4^-$ and $Al_2Cl_7^-$ anions were present in the ionic liquid electrolyte at the molar ratio of about 2.78 (Supplementary Figure 27).[35] All the electrochemical measurements were

performed in the glove box. The galvanostatic electrochemical charge-discharge cycling of the artificial muscle was performed on a LAND G340A battery tester. The CV measurement and square wave voltage were performed on a CHI760E electrochemical workstation. The injected charge (Q) was calculated following:

$$Q = \int I dt \tag{1}$$

Where the I is the current, and t is the time.

The contraction length was recorded by a contactless electromagnetic sensor. The generated isometric stress (σ) of the yarn muscle was recorded by a load cell (JZ-101, XINHANG). Contractile strokes (ε) were characterized by a contactless electromagnetic sensor.

$$\sigma = \frac{F}{S} \tag{2}$$

$$\varepsilon = \frac{\Delta L}{L} \times 100\% \tag{3}$$

Where the F is the force measured by the load cell, S is the cross-sectional area, ΔL is the contraction length, and L is the original length of CNT yarn.

Ex-situ WAXS spectroscopy: The CNT yarns were prepared by applying a twist density of about 4600 turns m^{-1}. Then the yarns were charged and discharged to different states during the CV scan between 0 V to 2.2 V at 1 mV s^{-1}. After the reaction, the yarns were removed from the glove box and were annealed at 80 °C for 2 h. The ex-situ WAXS measurements were performed on a Xenocs Xeuss 3.0 laboratory beamline. An X-ray wavelength of λ=1.54189 Å and a beam size of (0.9×0.9) mm^2 were employed for the measurements. The scattered intensities were

collected using a Dectris EIGER2 R 1M detector with a sample to detector distance of 50 mm for WAXS measurements (instrument resolution of ~0.067 Å^{-1}).

In-situ Raman spectroscopy: The in-situ Raman spectroscopy was performed through a homemade reaction cell with a quartz window by using a HeNe laser with a wavelength of 633 nm (Renishaw in Via Qantor). The CNT yarn without coiled structure and the commercial aluminum sheet were used. The spectral data were collected during the CV scan between 0 V to 2.2 V at 0.6 mV s^{-1}.

High-resolution EDS measurements: The CNT coiled yarn was charged to 2.2 V by CV scan at 1 mV s^{-1}. The soaked yarn was obtained by soaking the CNT yarn into $AlCl_3$/EMICl ionic liquid electrolyte for 2 h. Then the CNT yarn muscles were washed with anhydrous methanol. The cross-sections of the CNT yarns were obtained by radially sectioning the CNT to a depth of 10 μm from the surface, which was using a focused ion beam operated at 30 kV (Thermo Fisher Helos 5 UX). And the TEM images and the high-resolution EDS elemental mapping images of the cross-section were obtained using Talos F200X (Thermo Fisher).
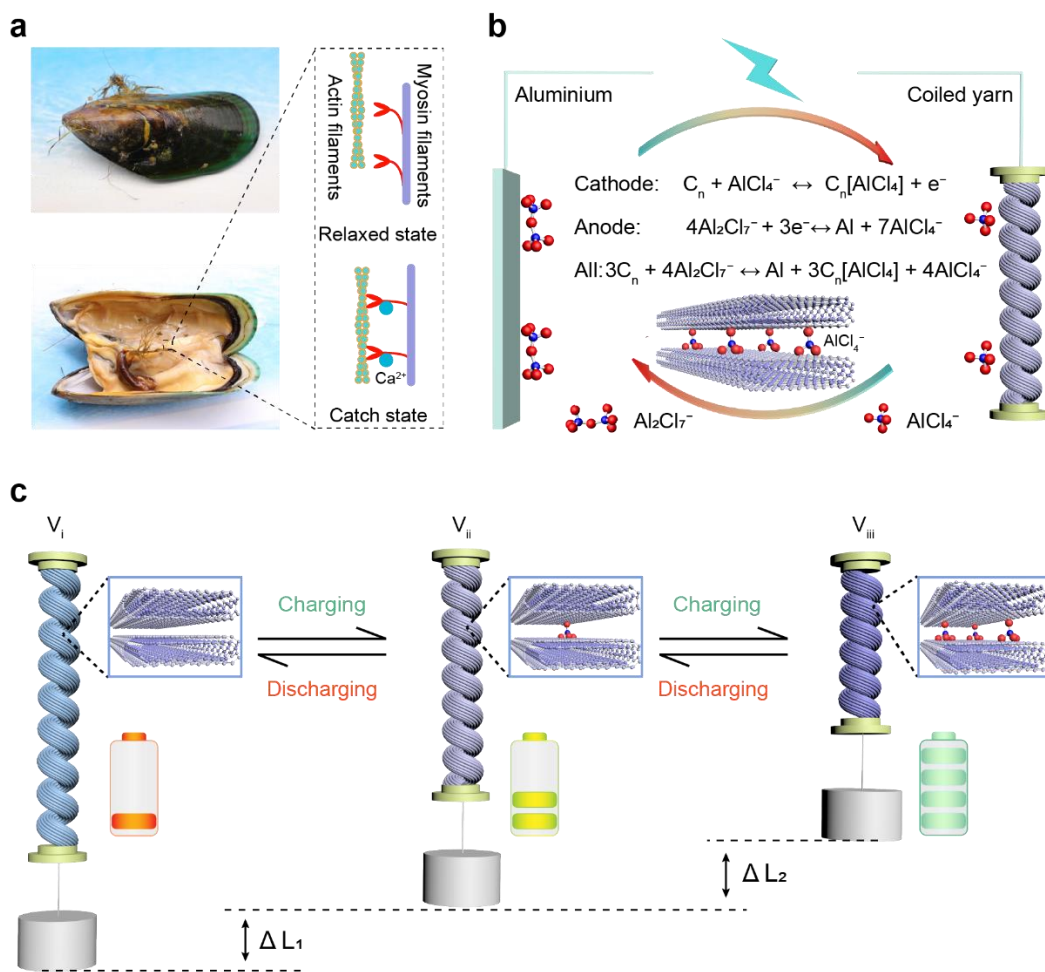
Figure 1. Schematic illustration of mussel-inspired artificial muscle with catch state and stepwise actuation. (a) The catch state of the mussel and the simplified mechanism (insert). (b) The structural and reaction equations of the actuation system consisted of an Al thin plate, a CNT coiled yarn, and an $AlCl_3$/[EMIm]Cl ionic liquid electrolyte. (c) Actuation process showing stepwise actuation and catch state during a CNT coiled yarn charged at different capacity levels.
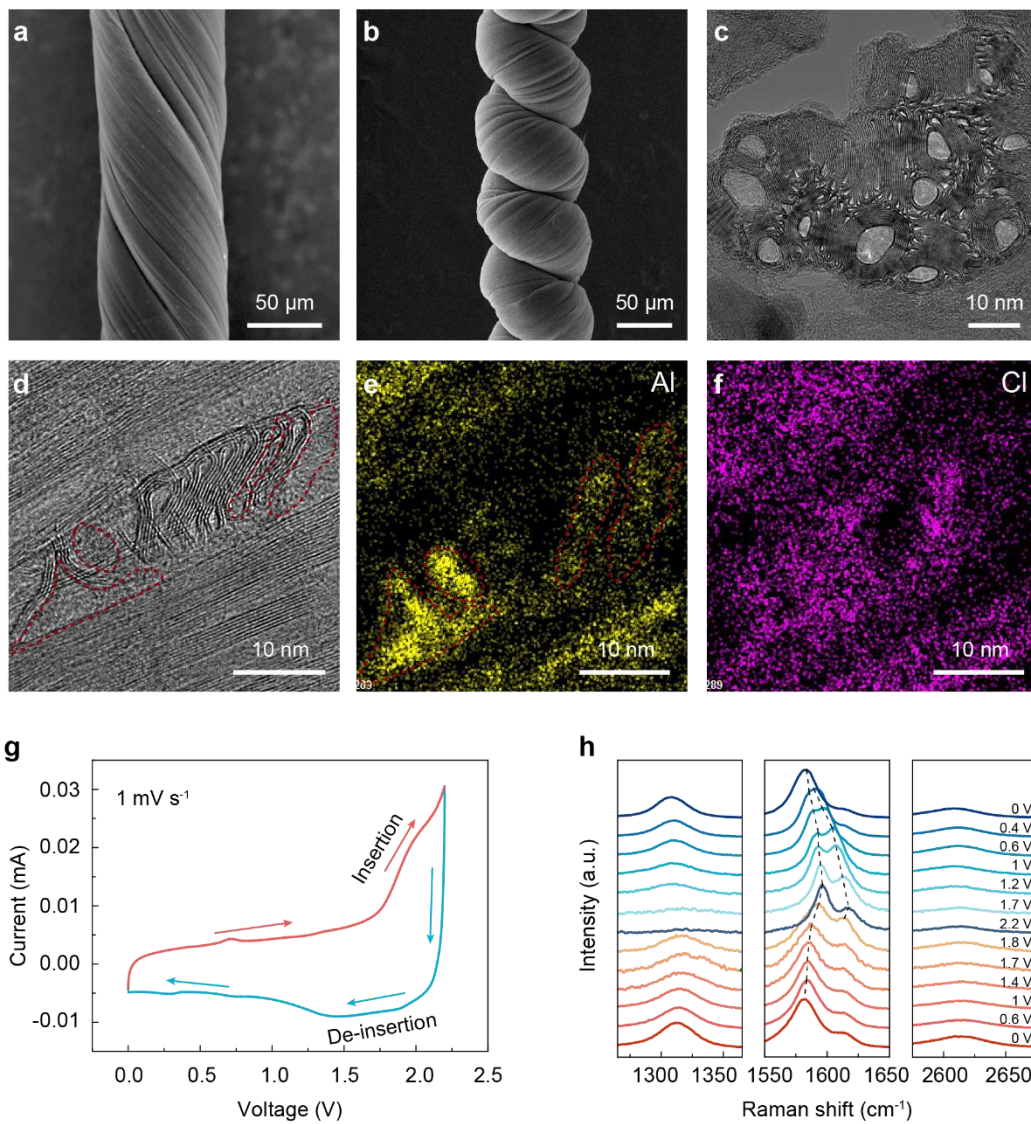
Figure 2. Ion insertion and extraction in artificial muscles. SEM images of pristine twisted CNT yarn (a) and fully coiled CNT yarn (b). (c) TEM image of the cross-section of pristine CNT coiled yarn showing collapsed CNTs in a bundle. (d) TEM image of the cross-section of full charged CNT coiled yarn. (e, f) High-resolution EDS elemental mapping image of Al (e) and Cl (f). (g) The second cycled CV curve of coiled CNT yarn was carried out at 1 mV s^{-1} between 0 V to 2.2 V versus Al plate. (h) In-situ Raman spectroscopy was recorded on CNT yarn during CV scanning at 0.6 mV s^{-1}.
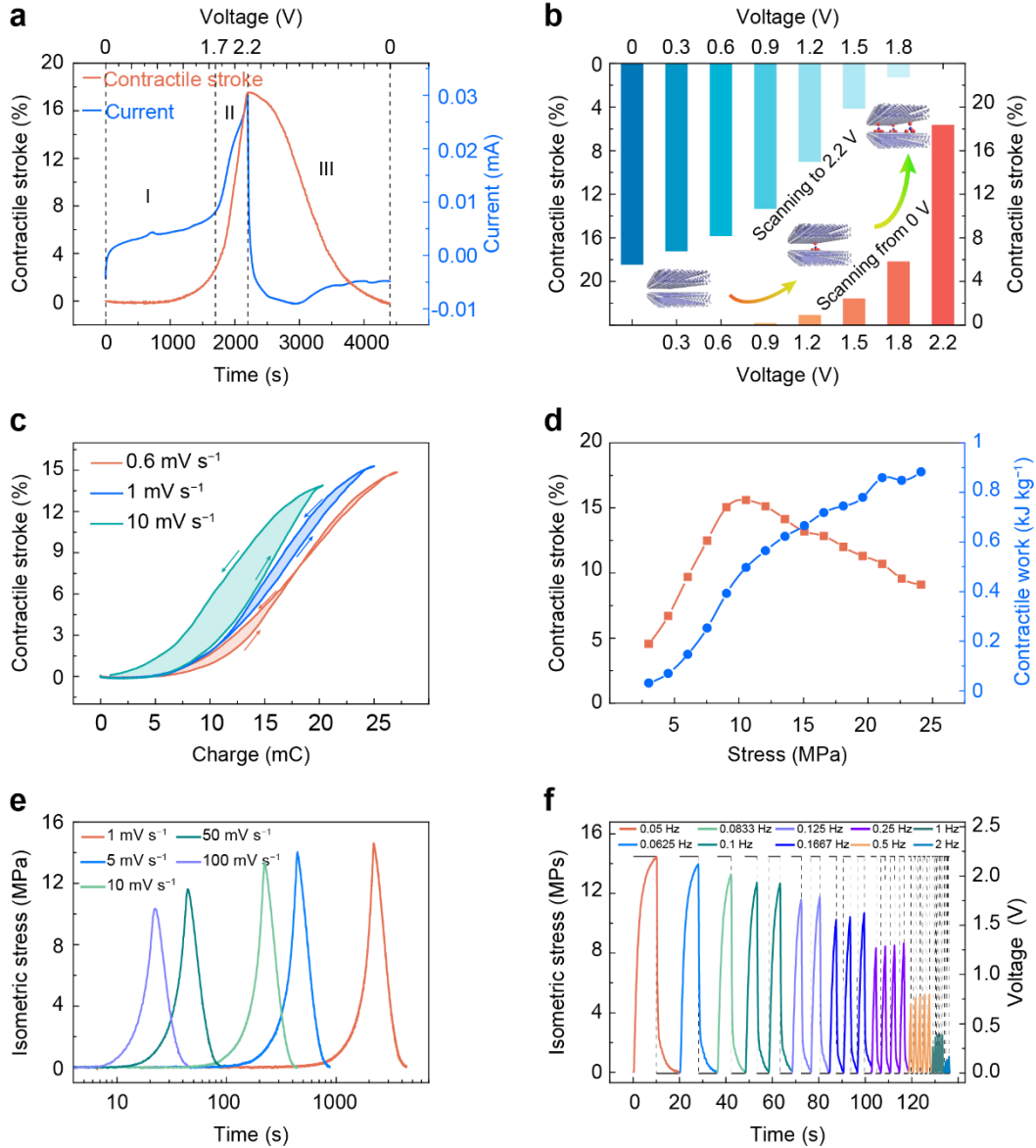
Figure 3. Electrochemical actuation performance of artificial yarn muscles by aluminum-ion intersection and extraction. (a) Contractile stroke and current versus time during a full CV scan between 0 V to 2.2 V at 1 mV s^{-1} for a coiled yarn bearing 12.1 MPa applied stress. The corresponding voltage profile was shown on the top x-axis. (b) The contractile stroke of the yarn muscle at different voltage windows at a scan rate of 1 mV s^{-1} using 12.1 MPa applied stress, inset shows the distribution of the ions at different stages. (c) The charge dependence of contractile stroke at different scan rates using 12.1 MPa applied stress. (d) The effect of stress on the

contractile stroke and actuation work during the CV scan under the electrochemical window of 0 V to 2.2 V and 10 mV s^{-1} scan rate. (e) The generated isometric stress versus scan rate during CV scan between 0 V to 2.2 V under 12.1 MPa applied stress. (f) The isometric stress curves under different on/off frequencies when a 0 V to 2.2 V square wave and tension stress of 12.1 MPa were applied.
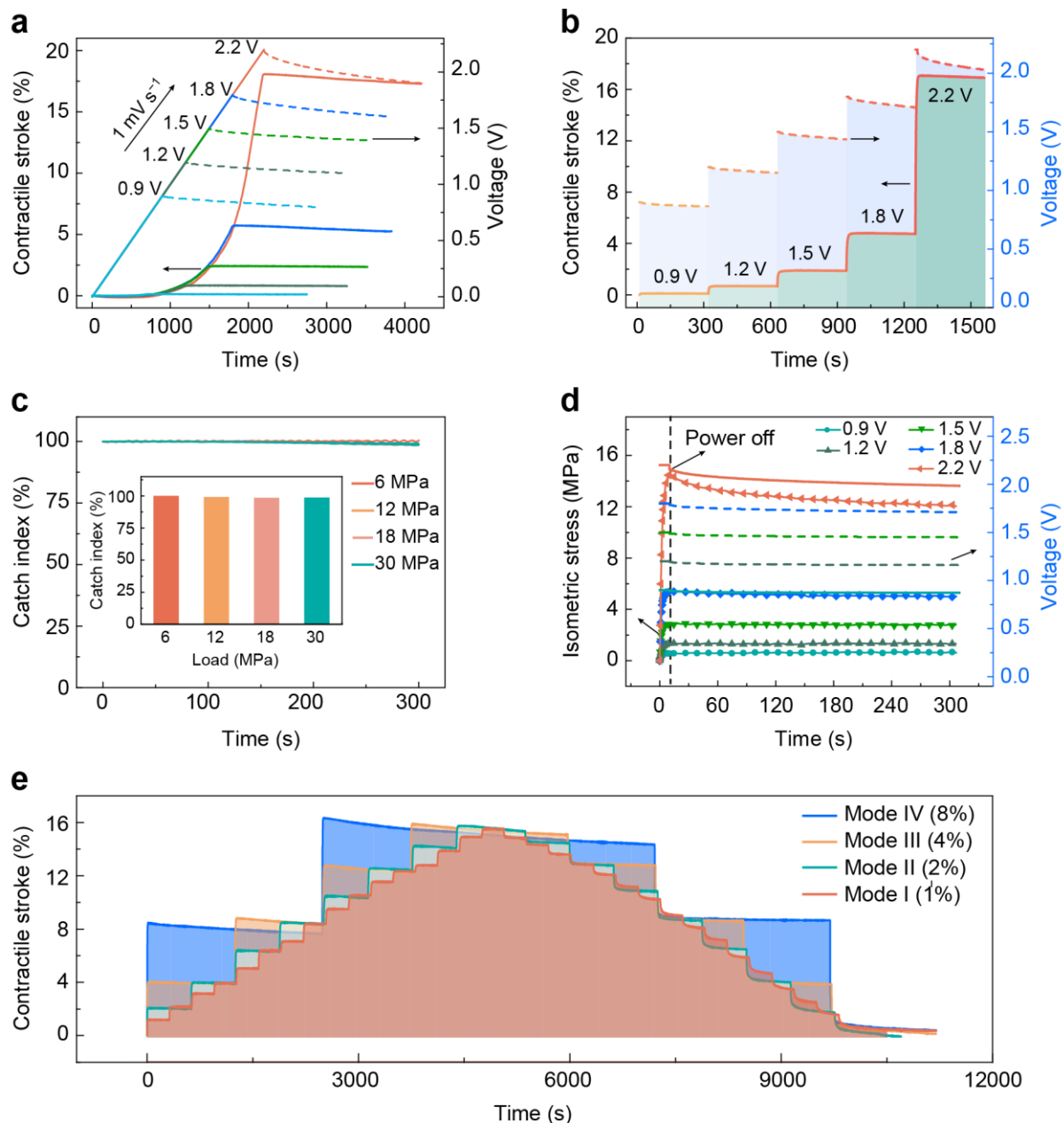
Figure 4. Energy-free high-tension catch state and programmable stepwise actuation of artificial muscles. (a) The contractile stroke and the applied voltage (solid line) and the recorded open-circuit voltage (dash line) between the yarn muscle and the Al plate versus time, during voltage sweeping from 0 V at 1 mV s−1 to target voltages and then powered off for 2000 s. The tension applied to the muscle is 12.1 MPa. (b) The contractile stroke and the open-circuit voltage between the yarn muscle and the Al plate versus time. Different voltages were applied for 10 s and then

turned off for 300 s. The tension applied to the muscle is 12.1 MPa. (c) The time dependence of the catch index of the yarn muscle under different tension loads when the applied power was turned off. The inset is the relationship between the catch indexes after power off for 300 s and the applied tension. (d) The generated isometric stress and the applied voltage (solid line) and the recorded open-circuit voltage (dash line) between the yarn muscle and the Al plate versus time, when voltages were applied for 10 s and then turned off for 300 s. The tension applied to the muscle is 12.1 MPa. (e) The programmable stepwise actuation at stroke steps of 8%, 4%, 2%, and 1%. The utilized voltages were applied for 10 s. The tension applied to the muscle is 12.1 MPa.
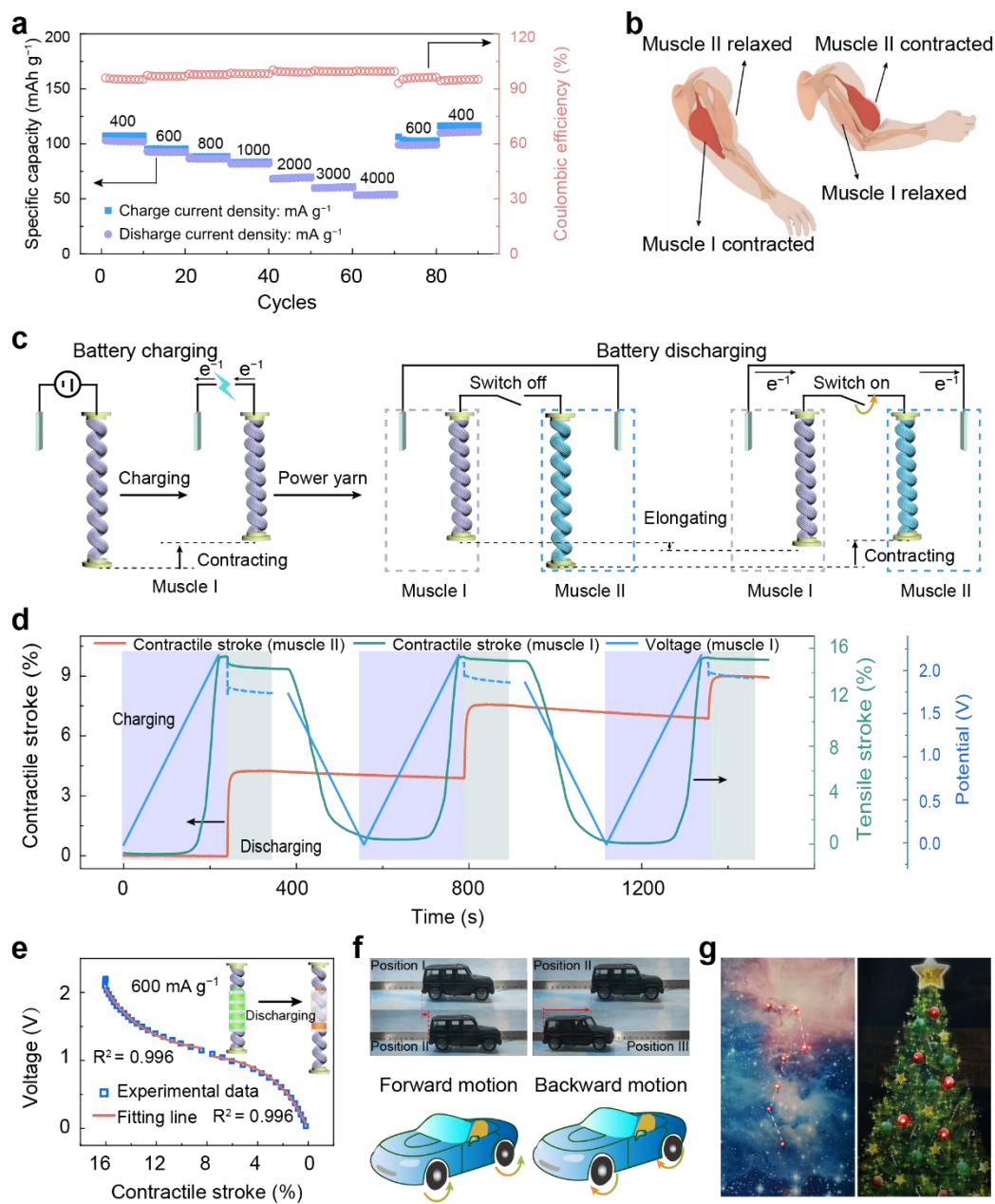
Figure 5. Energy storage of artificial muscle and the application demonstration. (a) Galvanostatic charge and discharge capacities and Coulombic efficiency at different current densities. (b) Diagram of contraction/extension of muscle I (biceps) and muscle II (triceps) when the arm was flexed and extended. (c) Schematic illustration of the contracted artificial muscle (muscle I) serves as a battery to power the other artificial muscle (muscle II). (d) The contractile stroke versus time

during using muscle I (contracted yarn) to power muscle II. (e) The experimental and fitting curves of voltage versus contractile stroke, when the artificial muscle was discharged at a current density of 0.6 A g^{-1}, and the inset displays the schematic illustration of the relationship between voltage and contractile stroke. (f) The use of Artificial muscle to power a car toy to go forward and turn back. (g) The LED patterns of the Big Dipper and Christmas trees are powered by artificial muscles.

ASSOCIATED CONTENT

Supporting Information.

Figure S1–Figure S27, and Table S1–Table S2 are shown in the supporting information file. Supporting Movies (Video S1 and Video S2) are available from the Online Library or from the author.

AUTHOR INFORMATION

Corresponding Author

E-mail: jtdi2009@sinano.ac.cn, qwli2007@sinano.ac.cn

Author Contributions

J.D. conceived the research. M. R., Y. W., and L. D. carried out the experiments. M. R., Y. Z., P. X., X. W., J. D., and Q. L. analyzed the experimental data. M. R. and J. D. wrote the manuscript. All authors discussed the results and revised the manuscript.

Notes

The authors declare no competing financial interest

REFERENCES

(1)   Yamada, A.; Yoshio, M.; Nakamura, A.; Kohama, K.; Oiwa, K., Protein Phosphatase 2B Dephosphorylates Twitchin, Initiating the Catch State of Invertebrate Smooth Muscle. J. Biol. Chem. 2004, 279 (39), 40762-40768.

(2)   Sugi, H.; Ohno, T.; Moriya, M., Mechanism and Function of the Catch State in Molluscan Smooth Muscle: A Historical Perspective. Int. J. Mol. Sci. 2020, 21 (20).

(3)   Li, M.; Pal, A.; Aghakhani, A.; Pena-Francesch, A.; Sitti, M., Soft actuators for real-world applications. Nat. Rev. Mater. 2022, 7 (3), 235-249.

(4)   Cianchetti, M.; Laschi, C.; Menciassi, A.; Dario, P., Biomedical applications of soft robotics. Nat. Rev. Mater. 2018, 3 (6), 143-153.

(5)   Apsite, I.; Salehi, S.; Ionov, L., Materials for Smart Soft Actuator Systems. Chem. Rev. 2022, 122 (1), 1349-1415.

(6)   Mirvakili, S. M.; Hunter, I. W., Artificial Muscles: Mechanisms, Applications, and Challenges. Adv. Mater. 2018, 30 (6), 1704407.

(7)   Xiong, J.; Chen, J.; Lee, P. S., Functional Fibers and Fabrics for Soft Robotics, Wearables, and Human–Robot Interface. Adv. Mater. 2021, 33 (19), 2002640.

(8)   Haines, C. S.; Lima, M. D.; Li, N.; Spinks, G. M.; Foroughi, J.; Madden, J. D. W.; Kim, S. H.; Fang, S.; Jung de Andrade, M.; Göktepe, F.; Göktepe, Ö.; Mirvakili, S. M.; Naficy, S.; Lepró, X.; Oh, J.; Kozlov, M. E.; Kim, S. J.; Xu, X.; Swedlove, B. J.; Wallace, G. G.; Baughman, R. H., Artificial Muscles from Fishing Line and Sewing Thread. Science 2014, 343 (6173), 868–872.

(9)   Yuan, J.; Neri, W.; Zakri, C.; Merzeau, P.; Kratz, K.; Lendlein, A.; Poulin, P., Shape memory nanocomposite fibers for untethered high-energy microengines. Science 2019, 365 (6449), 155.

(10)   Kanik, M.; Orguc, S.; Varnavides, G.; Kim, J.; Benavides, T.; Gonzalez, D.; Akintilo, T.; Tasan, C. C.; Chandrakasan, A. P.; Fink, Y.; Anikeeva, P., Strain-programmable fiber-based artificial muscle. Science 2019, 365 (6449), 145–150.

(11)   Pelrine, R.; Kornbluh, R.; Pei, Q.; Joseph, J., High-Speed Electrically Actuated Elastomers with Strain Greater Than 100%. Science 2000, 287 (5454), 836-839.

(12)   Qiu, Y.; Zhang, E.; Plamthottam, R.; Pei, Q., Dielectric Elastomer Artificial Muscle: Materials Innovations and Device Explorations. Acc. Chem. Res. 2019, 52 (2), 316-325.

(13)   Zhang, Q. M.; Li, H.; Poh, M.; Xia, F.; Cheng, Z. Y.; Xu, H.; Huang, C., An all-organic composite actuator material with a high dielectric constant. Nature 2002, 419 (6904), 284-287.

(14)   Chu, H. T.; Hu, X. H.; Wang, Z.; Mu, J. K.; Li, N.; Zhou, X. S.; Fang, S. L.; Haines, C. S.; Park, J. W.; Qin, S.; Yuan, N. Y.; Xu, J.; Tawfick, S.; Kim, H.; Conlin, P.; Cho, M.; Cho, K.; Oh, J.; Nielsen, S.; Alberto, K. A.; Razal, J. M.; Foroughi, J.; Spinks, G. M.; Kim, S. J.; Ding, J. N.; Leng, J. S.; Baughman, R. H., Unipolar stroke, electroosmotic pump carbon nanotube yarn muscles. Science 2021, 371 (6528), 494–498.

(15)   Chen, P.; Xu, Y.; He, S.; Sun, X.; Pan, S.; Deng, J.; Chen, D.; Peng, H., Hierarchically arranged helical fibre actuators driven by solvents and vapours. Nat. Nanotechnol. 2015, 10 (12), 1077–1083.

(16)   Yu, K.; Ji, X.; Yuan, T.; Cheng, Y.; Li, J.; Hu, X.; Liu, Z.; Zhou, X.; Fang, L., Robust Jumping Actuator with a Shrimp-Shell Architecture. Adv. Mater. 2021, 33 (44), e2104558.

(17)   Mu, J.; Jung de Andrade, M.; Fang, S.; Wang, X.; Gao, E.; Li, N.; Kim, S. H.; Wang, H.; Hou, C.; Zhang, Q.; Zhu, M.; Qian, D.; Lu, H.; Kongahage, D.; Talebian, S.; Foroughi, J.; Spinks, G.; Kim, H.; Ware, T. H.; Sim, H. J.; Lee, D. Y.; Jang, Y.; Kim, S. J.; Baughman, R. H., Sheath-run artificial muscles. Science 2019, 365 (6449), 150–155.

(18)   Mirvakili, S. M.; Hunter, I. W., Multidirectional Artificial Muscles from Nylon. Adv. Mater. 2017, 29 (4), 1604734.

(19)   Acome, E.; Mitchell, S. K.; Morrissey, T. G.; Emmett, M. B.; Benjamin, C.; King, M.; Radakovitz, M.; Keplinger, C., Hydraulically amplified self-healing electrostatic actuators with muscle-like performance. Science 2018, 359 (6371), 61–65.

(20)   Chen, Y.; Zhao, H.; Mao, J.; Chirarattananon, P.; Helbling, E. F.; Hyun, N.-s. P.; Clarke, D. R.; Wood, R. J., Controlled flight of a microrobot powered by soft artificial muscles. Nature 2019, 575 (7782), 324-329.

(21)   Rothemund, P.; Kellaris, N.; Mitchell, S. K.; Acome, E.; Keplinger, C., HASEL Artificial Muscles for a New Generation of Lifelike Robots-Recent Progress and Future Opportunities. Adv. Mater. 2021, 33 (19), e2003375.

(22)   Cheng, H.; Hu, Y.; Zhao, F.; Dong, Z.; Wang, Y.; Chen, N.; Zhang, Z.; Qu, L., Moisture-Activated Torsional Graphene-Fiber Motor. Adv. Mater. 2014, 26 (18), 2909-2913.

(23)   Gong, J.; Lin, H.; Dunlop, J. W. C.; Yuan, J., Hierarchically Arranged Helical Fiber Actuators Derived from Commercial Cloth. Adv. Mater. 2017, 29 (16), 1605103.

(24)   Lima, M. D.; Hussain, M. W.; Spinks, G. M.; Naficy, S.; Hagenasr, D.; Bykova, J. S.; Tolly, D.; Baughman, R. H., Efficient, Absorption-Powered Artificial Muscles Based on Carbon Nanotube Hybrid Yarns. Small 2015, 11 (26), 3113-8.

(25)   Kim, O.; Kim, H.; Choi, U. H.; Park, M. J., One-volt-driven superfast polymer actuators based on single-ion conductors. Nat. Commun. 2016, 7 (1), 13576.

(26)   Madden, J. D. W.; Vandesteeg, N. A.; Anquetil, P. A.; Madden, P. G. A.; Takshi, A.; Pytel, R. Z.; Lafontaine, S. R.; Wieringa, P. A.; Hunter, I. W., Artificial muscle technology: physical principles and naval prospects. IEEE J. Oceanic Eng. 2004, 29 (3), 706–728.

(27)   Lin, M.-C.; Gong, M.; Lu, B.; Wu, Y.; Wang, D.-Y.; Guan, M.; Angell, M.; Chen, C.; Yang, J.; Hwang, B.-J.; Dai, H., An ultrafast rechargeable aluminium-ion battery. Nature 2015, 520 (7547), 324-328.

(28)   Tu, J.; Song, W.-L.; Lei, H.; Yu, Z.; Chen, L.-L.; Wang, M.; Jiao, S., Nonaqueous Rechargeable Aluminum Batteries: Progresses, Challenges, and Perspectives. Chem. Rev. 2021, 121 (8), 4903–4961.

(29)   Hainesa, C. S.; Li, N.; Spinksb, G. M.; Alieva, A. E.; Di, J.; Baughmana, R. H., New twist on artificial muscles. Proc. Natl. Acad. Sci. U. S. A. 2016, 113 (11), 11709–11716.

(30)   Li, Y. L.; Kinloch, I. A.; Windle, A. H., Direct Spinning of Carbon Nanotube Fibers from Chemical Vapor Deposition Synthesis. Science 2004, 304 (5668), 276–278.

(31)   Drozdov, G.; Xu, H.; Frauenheim, T.; Dumitrică, T., Densely-packed bundles of collapsed carbon nanotubes: Atomistic and mesoscopic distinct element method modeling. Carbon 2019, 152, 198-205.

(32)   Liu, Z.; Wang, J.; Ding, H.; Chen, S.; Yu, X.; Lu, B., Carbon Nanoscrolls for Aluminum Battery. ACS Nano 2018, 12 (8), 8456-8466.

(33)   Meshot, E. R.; Zwissler, D. W.; Bui, N.; Kuykendall, T. R.; Wang, C.; Hexemer, A.; Wu, K. J. J.; Fornasiero, F., Quantifying the Hierarchical Order in Self-Aligned Carbon Nanotubes from Atomic to Micrometer Scale. ACS Nano 2017, 11 (6), 5405-5416.

(34)   Boaretto, N.; Rana, M.; Marcilla, R.; Vilatela, J. J., Revealing the Mechanism of Electrochemical Lithiation of Carbon Nanotube Fibers. ACS Appl. Energy Mater. 2020, 3 (9), 8695-8705.

(35)   Angell, M.; Pan, C. J.; Rong, Y. M.; Yuan, C. Z.; Lin, M. C.; Hwang, B. J.; Dai, H. J., High Coulombic efficiency aluminum-ion battery using an AlCl3-urea ionic liquid analog electrolyte. Proc. Natl. Acad. Sci. U. S. A. 2017, 114 (5), 834-839.

(36)   Kim, Y. A.; Kojima, M.; Muramatsu, H.; Umemoto, S.; Watanabe, T.; Yoshida, K.; Sato, K.; Ikeda, T.; Hayashi, T.; Endo, M.; Terrones, M.; Dresselhaus, M. S., In situ Raman study on single- and double-walled carbon nanotubes as a function of lithium insertion. Small 2006, 2 (5), 667-76.

(37)   Baughman, R. H.; Cui, C.; Zakhidov, A. A.; Iqbal, Z.; Barisci, J. N.; Spinks, G. M.; Wallace, G. G.; Mazzoldi, A.; De Rossi, D.; Rinzler, A. G.; Jaschinski, O.; Roth, S.; Kertesz, M., Carbon Nanotube Actuators. Science 1999, 284, 1340–1344.

(38)   Mirfakhrai, T.; Madden, J. D. W.; Baughman, R. H., Polymer artificial muscles. Mater. Today 2007, 10 (4), 30-38.

(39)   Ren, M.; Qiao, J.; Wang, Y.; Wu, K.; Dong, L.; Shen, X.; Zhang, H.; Yang, W.; Wu, Y.; Yong, Z.; Chen, W.; Zhang, Y.; Di, J.; Li, Q., Strong and Robust Electrochemical Artificial Muscles by Ionic-Liquid-in-Nanofiber-Sheathed Carbon Nanotube Yarns. Small 2021, 17 (5), 2006181.

(40)   Qiao, J.; Di, J.; Zhou, S.; Jin, K.; Zeng, S.; Li, N.; Fang, S.; Song, Y.; Li, M.; Baughman, R. H.; Li, Q., Large-Stroke Electrochemical Carbon Nanotube/Graphene Hybrid Yarn Muscles. Small 2018, 14 (38), 1801883.

(41)   Mirvakili Seyed, M.; Sim, D.; Hunter Ian, W.; Langer, R., Actuation of untethered pneumatic artificial muscles and soft robots using magnetically induced liquid-to-gas phase transitions. Sci. Robot. 2020, 5 (41), eaaz4239.

(42)   Kellaris, N.; Rothemund, P.; Zeng, Y.; Mitchell, S. K.; Smith, G. M.; Jayaram, K.; Keplinger, C., Spider-Inspired Electrohydraulic Actuators for Fast, Soft-Actuated Joints. Adv. Sci. 2021, 8 (14), e2100916.

(43)   Noh, M.-S.; Lee, H.; Song, Y. G.; Jung, I.; Ning, R.; Paek, S. W.; Song, H.-C.; Baek, S.-H.; Kang, C.-Y.; Kim, S., Li alloy-based non-volatile actuators. Nano Energy 2019, 57, 653-659.

(44)   Kim, S. H.; Haines, C. S.; Li, N.; Kim, K. J.; Mun, T. J.; Choi, C.; Di, J.; Oh, Y. J.; Oviedo, J. P.; Bykova, J.; Fang, S.; Jiang, N.; Liu, Z.; Wang, R.; Kumar, P.; Qiao, R.; Priya, S.; Cho, K.; Kim, M.; Lucas, M. S.; Drummy, L. F.; Maruyama, B.; Lee, D. Y.; Lepró, X.; Gao, E.; Albarq, D.;

Ovalle-Robles, R.; Kim, S. J.; Baughman, R. H., Harvesting electrical energy from carbon nanotube yarn twist. Science 2017, 357 (6353), 773–778.

(45)   Seong, W. M.; Park, K.-Y.; Lee, M. H.; Moon, S.; Oh, K.; Park, H.; Lee, S.; Kang, K., Abnormal self-discharge in lithium-ion batteries. Energy Environ. Sci. 2018, 11 (4), 970-978.

(46)   Lee, J. A.; Li, N.; Haines, C. S.; Kim, K. J.; Lepro, X.; Ovalle-Robles, R.; Kim, S. J.; Baughman, R. H., Electrochemically Powered, Energy-Conserving Carbon Nanotube Artificial Muscles. Adv. Mater. 2017, 29 (31), 1700870.
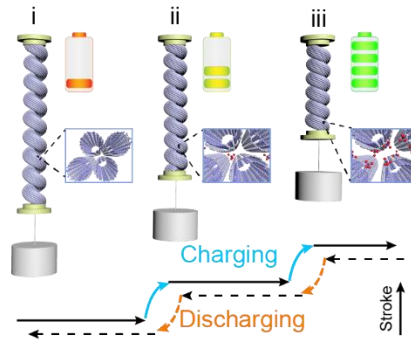
A new strategy that utilizes an electrochemically reversible insertion reaction to achieve an energy-free high-tension catch state and programmable stepwise actuation in the carbon nanotube yarn muscle is proposed. Importantly, the yarn muscle with a high capacity can be utilized as a battery to power secondary muscles or other devices.